CrystEngComm

Accepted Manuscript

ROYAL SOCIETY OF CHEMISTRY

www.rsc.org/crystengcomm

One-pot synthesis of Zn-doped SnO_2 nanosheet-based hierarchical architectures as glycol gas sensor and photocatalyst

Qinqin Zhao[1], Xiaolong Deng[1], Meng Ding[1], Lin Gan[2], Tianyou Zhai[2], Xijin Xu[1]**

[1] School of Physics and Technology, University of Jinan, 336 Nanxinzhuang West Road, Jinan 250022, Shandong, P. R. China

[2] State Key Laboratory of Material Processing and Die & Mould Technology, School of Materials Science and Engineering, Huazhong University of Science and Technology (HUST), Wuhan 430074, Hubei, P. R. China

Abstract: Zn-doped SnO_2 hierarchical architectures (ZSHAs) with controllable size have been prepared using a facile hydrothermal method, which are composed of two dimensional (2D) nanosheets with the thickness of about 40 nm. The properties of ZSHAs have been explored by gas sensing and photocatalytic test, respectively. The sensor response ($S = R_a/R_g$) can reach to be 43 at 100 ppm glycol, and the detection limit can be down to 5 ppm-level with a response about 5, combined with a low operation temperature of 240 ^oC, suggesting a promising application of ZSHAs in glycol gas sensing. Besides, the photocatalytic activities of ZSHAs have been evaluated by the degradation measurement of methylene blue (MB), methylene orange (MO), and rhodamine B (RhB), respectively. As a result, the ZSHAs demonstrate a much higher selectivity on the degradation of MB (91%) than that of MO (40%) and RhB (60%) in 60 min measurement.

Keywords: SnO_2, Zn-doping, Hierarchical architectures, Gas sensor, Photocatalysis

1. Introduction

Environmental issues have become research focus for years. Semiconducting oxide nanocrystals of controllable dimensions and compositions have been intensively studied in the fields of catalytically decomposing and detecting volatile and toxic organic compounds.[1,2] It is widely accepted that both photocatalytic and gas sensing reactions generally occurred on the materials surfaces based on the adsorption-reaction-desorption process.[3-6] Therefore, a large specific surface area of would be beneficial because of containing more active sites on surface. [6] Furthermore, defects such as oxygen vacancies can induce trapping states and thus inhibit the recombination of electron-hole pairs by capturing electrons alone in photocatalysis [6-8] and adsorb more target gas molecules in gas sensing.[9] As a typical wide band gap n-type semiconductor (3.6 eV), tin oxide (SnO_2) [10-13] becomes an attraction in the application of gas sensing due to its low cost, high sensitivity, fast gas response, high mobility of conducting electrons, and good chemical and thermal stability.[14] Besides, it has also been used as photocatalyst because of its unique optical, catalytic, and electrical properties.[15] Generally, the effective surface areas and surface defects concentration dictate the final performance of active materials, which are in turn greatly affected by the morphologies and structures of materials.[16] Thus, considerable efforts have been devoted to synthesize different SnO_2 nanoarchitectures, such as nanosheets,[6] nanorods[17,18] and hierarchical architectures.[12] In particular, hierarchical SnO_2 structures features all desirable characteristics for gas sensor and photocatalysis. [6,17,19] For example, Wang et al.[20] synthesized ultrathin SnO_2 nanowires structures which exhibited relative low response. Fan et al.[21] prepared coral SnO_2 nanoparticles and found them possessing improved photocatalytic performance toward MO. However, the low sensing response (R_a/R_g) or long degradation time inhibit their

potential applications.

Recently, it has been widely reported that doping SnO_2 with certain dopants, such as Cu,[22] Pt,[23] Zn,[24,25,26] and Co,[27] improves both the sensitivity of SnO_2 in gas sensing and photocatalytic activity[22] and modulates the morphologies of SnO_2 simultaneously.[28] Among these, Zn doping SnO_2[24,25] is the most attractive focus due to the similar ion radius but different charge numbers of Zn^{2+} and Sn^{4+} (0.074 nm for Zn^{2+}, 0.071 nm for Sn^{4+}). Similar ion radius ensure the lattice integrity of SnO_2 after doping and for the different charge numbers, oxygen vacancies will be generated for charge compensation in SnO_2. Therefore, Zn-doped SnO_2 hierarchical architectures (ZSHAs) would expect to exhibit excellent gas sensing and photocatalytic properties. However, the synthesis procedures of hierarchical pure and doped SnO_2 nanostructures, previously, were relatively complex, worse, accompanying with the inevitable pollutions.[29] Thus, it is necessary to explore new ways for simplification of pure and doped SnO_2 hierarchical architectures synthesis.

In this paper, we demonstrated a simple novel hydrothermal method for ZSHAs synthesis. The ZSHAs, composed of a number of 2D nanosheets, exhibit excellent sensitivity and selectivity to glycol, in which a high detection response, 43, have been achieved under 100 ppm glycol and the detecting limit can be lowered to 5 ppm at detection response of 5. In addition, the operating temperature is down to be 240 °C. Moreover, the photocatalytic properties of ZSHAs have been evaluated by the degradation test of MB, MO, and RhB under UV light irradiation. A high photocatalytic degradation selectivity of ZSHAs on MB (91%), contrasted with on MO (40%) and RhB (60%), has been observed in 60 min measurement.

2 Experimental

Synthesis of ZSHAs: All chemicals were of analytical grade regents without any

further purification. A typical synthesis process was as follows[19]: 4 mmol $SnCl_2 \cdot 2H_2O$, 10 mmol $Na_3C_6H_5O_7 \cdot 2H_2O$ and 4 mmol NaOH were dissolved in a mixture of 30 ml ethanol and 45 ml deionized water with vigorous stirring to form homogeneous solution. Then, 0.2 mmol $Zn(NO_3)_2 \cdot 6H_2O$ was added into above solution under ultrasonication. Afterward, the mixed solution was transferred into the Teflon-lined stainless steel autoclave, and kept at 180 ^oC for 16 h. After reaction, the obtained precipitates were collected by centrifugation and washed several times with deionized water and ethanol. Finally, the sample was dried at 60 ^oC in air for 12 h and annealed at 600 ^oC for 2 h.

Material Characterizations: The samples were characterized by a field emission scanning electron microscope (FESEM, FEI QUANTA FEG250) equipped with an energy dispersive x-ray spectroscopy (EDX, INCA MAX-50), high-resolution transmission electron microscope (HRTEM, JEM-2100F), X-ray diffraction (XRD, D8-Advance, Bruker) with Cu K_α radiation.

Gas-Sensing Measurements: Gas sensors were fabricated as follows: In brief, the paste of obtained sample was coated onto an Al_2O_3 tube to form thick film between two parallel Au electrodes. A Ni-Cr coil heater was used to keep the sensor at operating temperature. The gas sensor properties were measured by gas sensing test system (WS-30A, Weisheng Electronics, Zhengzhou, China) under laboratory conditions (30% ± 10% RH, 23 ± 1 °C) as shown in Fig. 1(a). The schematic electronic circuit of test system was shown in Fig. 1 (b). In the circuit, V_H is the heating voltage, R_L is a constant resistance (4.7 MΩ), V_{RL} is the voltage on R_L and V_C is constant voltage (5 V) which was applied on the R_L and the sensor. A given amount of target gas was injected into the test chamber, when the response reached a constant value, the upper cover was removed and the sensor began to recover. The response

was defined as $S = R_a/R_g$ for target gas, where R_a and R_g are the sensor resistances in air and in target gas, respectively.

Photocatalytic Measurements: Photocatalytic degradations of organic dyes (MB, MO and RhB) were carried out in the presence of the products as photocatalysts under the mercury lamp (500 W) illumination. Generally, 0.1 g of sample was added in 50 mL organic dye aqueous solutions (10 mg L^{-1}). The solutions were stirred for 30 min in the dark to establish the adsorption-desorption equilibrium. Then, the solutions were exposed to UV irradiation. The photocatalytic degradation was estimated by measuring the absorbance of dye solution in the presence of photocatalyst at different time intervals. The degradation efficiencies of organic dyes were analyzed by monitoring the dye decolorization at the maximum absorption wavelength using UV-vis spectrophotometer (TU-1901).

3 Results and Discussion

The morphologies and structures of ZSHAs are shown in Fig. 2. The typical low magnification SEM image (Fig. 2a) shows that the products are mostly clusters structures, which are composed of Zn-doped SnO_2 nanosheets (40 nm) with a relatively rough surface (Fig. 2b). TEM image (Fig. 2c) indicates the nanosheets structures, and its HRTEM image (Fig. 2d) confirms its single crystalline feature with the lattice spacing of 0.34 nm, corresponding to the (110) lattice planes. EDX analysis (Fig. 2e) demonstrates that the nanosheet structures are composed of Zn, Sn and O elements. The peak corresponding to C comes from conducting resin. The XRD patterns (Fig. 2f) indicates that all the diffraction peaks could be well indexed to the tetragonal rutile structure of SnO_2, matching well with JCPDS card NO. 41-1445.

Glycol is one of the most important organic solvent, which is toxic and can cause great damage on human health.[30] Glycol contains hydroxyl group, which will be

oxidized into glycolic acid and then into oxalic acid with their working temperature of 80-90 ^{o}C. It exhibits a great damage on health, such as respiratory difficulty and pulmonary edema. It also affects the nervous system and even causes death. However, gas sensors for glycol detecting are rarely reported. Recently, Zhang et al.[31] fabricated porous SnO_2 nanotubes sensor to detect glycol while operating at 300 °C and the high operating temperature may inhibit their applications. In our work, Fig. 3a shows the response of ZSHAs at 100 ppm glycol, as a function of operating temperature in the range of 200-400 °C. It is observed that the response increases with the increment of working temperature before achieving maximum. The sensor exhibits maximum response of 43 at 100 ppm glycol at 240 °C, and then decreases as the temperature further increase, which can be explained by the competing desorption of chemisorbed oxygen.[32,33,34,35]. When the working temperature is higher than 240 ^{o}C, the oxygen chemically absorbed on the surface of the ZSHAs will gain enough energy to desorb from the surfaces, and then the chemical adsorption of oxygen gets saturation. With the increase of operating temperature, the rate of desorption is much higher than that of adsorption, limiting the reaction between adsorption oxygen and target gas molecules and further reducing response. The optimal operating temperature we reported here is down to be 240 ^{o}C, about 60 ^{o}C less than other previous reports, which can lead to lower power consumption.

Fig. 3b shows the dynamic response and recovery curve of Zn-doped SnO_2 sensor to glycol with variable concentrations from 5 ppm to 200 ppm at 240 °C. It can be clearly observed that the sensor responses increase with the increment of glycol concentrations. The gradually increased response reaches to 70 when the glycol concentration is 200 ppm. It also indicates that the detection limit can be down to 5 ppm-level with a response about 5. Generally, the relation between gas concentration

and response of metal–oxide-semiconductor (MOS) gas sensors can be described with an empirical formula as Eq. (1) and (2):

$$S = K_a[C]^{K_b} + 1 \quad (1)$$

$$\text{or} \quad \log(S-1) = K_b \log(C) + \log K_a \quad (2)$$

where K_a and K_b are constants and C is the concentration of target gas.[33,36] In our work, the response exhibits a good linear relationship with the concentration in a logarithm scale, as shown in Fig. 3c. Therefore, the detection limit of the sensor can be down to ppb-level in our case.[37]

The response-recovery behavior is also a vital characteristic parameter for gas sensors. It was defined as the time taken by the sensor to achieve 90% of the total resistance change in the case of adsorption and desorption, respectively.[32] It is observed that the response of Zn-doped SnO_2 sensor increased abruptly (40 s) after injection of target gas and need much longer time to recover to its initial value after the test gas was released, as shown in Fig. 3d. This may be attributed to the lower operating temperature (240 ^oC) which is not easy to break the bond between Zn-doped SnO_2 and glycol.[38] In addition, the hierarchical architectures may inhibit escape of glycol molecules, which also lead to a longer time recovery.

Selective detection of target gases remains a challenge and plays a major role in the applications of MOS-based gas sensors.[39] To identify their selectivity, the cross response properties were examined by exposing it to 100 ppm glycol and other gases like ethanol, acetone, benzene, paraxylene, water and hydrogen at 240 °C, as summarized in Fig. 4. It was seen that the response of Zn-doped SnO_2 sensor to 100 ppm glycol is much higher than those of other gases. The response can get up to 48, which was about four times higher than that of ethanol and more than ten times of other gases, indicating an excellent selectivity to glycol. The high response may be

ascribed to the high specific surface area. A comparison between the sensing performances of Zn-doped SnO_2 sensor and some others gas sensors previously reported is summarized in Table 1. As can be seen, the Zn-doped SnO_2 sensor has a lower working temperature and a higher response than others, which confirms that ZSHAs have an obvious advantage over others for glycol gas sensing.

As a typical n-type MOS, SnO_2-based sensors belong to the surface-controlled type, and the most widely accepted model is the formation of a charge depletion layer in the near-surface region of each grain.[32,33,41,42] The formation of oxygen adsorption induced electron depletion layer on SnO_2 grains surfaces, which played an important role in the sensing response.[41] The conductance of n-type semiconductor is determined by the amount of electrons in its conduction band. Based on the standard model,[42] when SnO_2 sensor is exposed to air, oxygen molecules will be adsorbed on its surface and further capture electrons from the conduction band to form oxygen ions (O_2^-, O^{2-}, O^-). It will form an electron depletion region on the surface of SnO_2, resulting in the increase of sensors resistance. Whereas when the sensors are exposed to reducing gas such as glycol or ethanol, the oxygen negative ions will react with target gas molecules and release the trapped electrons back to the conduction band of SnO_2. This reduces amount of surface adsorbed oxygen species, and leads to an increase of carrier concentrations of the sensors. Consequently, the depletion layer on the surface of sensors becomes thin, exhibiting a decrease of sensor resistance. Based on the formula of response ($S=R_a/R_g$), the response of sensor would be enhanced once switching from in air to in glycol or ethanol environment. As expected, the enhancement of response observed in Zn-doped SnO_2 sensor would be more apparent, which can be attributed to the following factors. Firstly, the grain size of SnO_2 will decrease with the doping of Zn, which may be ascribed to the pinning effect of defects

caused by doping.[43] Due to the above mentioned, the surfaces of SnO_2 nanosheets become more reactive and absorb more oxygen molecules to form ionized oxygen species.[44,45] Secondly, the specific surface area of Zn-doped SnO_2 is increased, which means that much more oxygen can be absorbed and ionized on surface of Zn-doped SnO_2. In addition, according to the solid state chemistry theory, the quantity of oxygen vacancies of Zn-doped SnO_2 architectures is also increased due to the substitution of Zn^{2+} for Sn^{4+}. Thus, owing to more oxygen species adsorbed on surface of SnO_2 and more surface oxygen vacancies in the Zn-doped SnO_2 architectures, the Zn-doped SnO_2 sensor shows a higher response.

Photocatalytic activities were evaluated by the degradation test of MB, MO and RhB, respectively. Fig. 5a shows the self-degradation adsorption spectrum of MB dye at different time intervals. The characteristic absorption peaks at 664 nm decrease slowly with the increasing of the illumination time. However, the absorption peak decreases quickly with the addition of ZSHAs catalysts (Fig. 5b). MB is degraded about 91% when the irradiation time is 60 min. However, the self-degradation of MB is only 20%, as shown in Fig. 5c. In order to illustrate the selectivity difference of ZSHAs among those dyes, the degradation efficiencies are compared for different dyes in 60 min as shown in Fig. 5d. The results show the degradation efficiencies of MB, MO, and RhB are about 92, 60, and 40% in 60 min, respectively. The changes in the organic pollutant concentrations under ultraviolet irradiation can be calculated as Eq. (3):

$$\mathrm{I} = \frac{C}{C_0} \times 100\% \qquad (3)$$

C_0 is the initial concentration of the organic pollutants, while the real time concentration of organic pollutants under ultraviolet light irradiation is expressed by C. The photocatalytic efficiency derived from the changes in the organic dye

concentration can be represented by the relative ratio C/C_0, which obviously demonstrates that ZSHAs have an excellent selectivity on photocatalytic degradation of MB dye.

The photocatalytic mechanism has been reported by some groups.[46-49] In general, hydroxyl radicals (•OH) play an important role in the photocatalytic degradation of dye molecules. Therefore, increasing the amount of •OH can enhance the photocatalytic efficiency. On the basis of the photocatalytic mechanism (Fig. 6), hydroxyl radicals (•OH) are generated from the oxidization of H_2O by photogenerated holes (h^+) under UV irradiation. When ZSHAs are irradiated, it is stimulated to produce h^+ and e^-. Then, h^+ are trapped by H_2O at the catalyst surface to yield hydroxyl radicals (•OH) with high oxidability and reactivity. Meanwhile, the rest e^- is absorbed by O_2 molecules attached on ZSHAs surface to form the oxygen radicals (O_2^-). The powerful oxidant, O_2^- and •OH can effectively decompose the organic dyes. Moreover, the catalyst interface and the defects caused by Zn doping can further inhibit the electron-hole recombination. Thus, the lifetime of excited electrons and holes is prolonged, inducing higher reaction efficiency. In brief, two ways benefit to the photocatalytic efficiency enhancement of Zn-doped SnO_2 nanosheet-based hierarchical architectures (ZSHAs). First, the longer lifetime of photogenerated electrons and holes induce higher concentration of radicals that promote the photocatalytic degradation of dyes. Second, more high-reactive sites can be accommodated by the novel ZSHAs. Here, the remarkable photocatalytic activities of Zn-doped SnO_2 architectures may be attributed to special hierarchical structure. The structure can provide more active sites to adsorb reactive species and O_2. It means that the hierarchical structure can improve the photon application efficiency,[6] which leads to a high photocatalytic efficiency.

These different degradation ratios may be attributed to the different molecular structures of the three dyes, which result in different degradation mechanisms. The high photocatalytic activity with MB may be attributed to the -N- bonds in MB and the sulfur involved in $=S^{+}-$ aromatic links in MB molecules which is more reactive than the sulfonyl group located on the p-benzene ring in MO molecules during the radical reactions. Additionally, the molecule of MB has a much smaller size than that of RhB, which is supposed to be easier to be absorbed and broken.[50]

4 Conclusions

In summary, a facile method has been developed for preparing Zn-doped SnO_2 hierarchical architectures consisted of interconnected nanosheets. The ZSHAs were used for high-sensitive and selective glycol gas sensors, in which the sensor response can reach to be 43, the detection limit can be down to 5 ppm-level and the operating temperature is down to be 240 °C. The ZSHAs were also used as an efficient photocatalyst for the degradation of MB, MO and RhB, in which the ZSHAs exhibited much higher degradation efficiency for MB (90%) than those of MO (40%) and RhB (60%). The substantial degradation of the dyes was mainly due to specific morphologies of ZSHAs in which high specific surface area and high concentration of oxygen vacancies were achieved simultaneously. This work demonstrates that Zn-doped SnO_2 nanosheet-based hierarchical architectures (ZSHAs) have a potential application in glycol gas sensor and photocatalytic degradation toward MB dye.

Acknowledgements

Thanks University of Jinan (UJn) for the support on new staff, and the project supported by the Taishan Scholar (No. TSHW20120210), the National Natural Science Foundation of China (Grant No. 11304120, 21322106, 51472097), Ministry

of Science and Technology of China (2015CB932600), the Encouragement Foundation for Excellent Middle-aged and Young Scientist of Shandong Province (Grant No. BS2012CL005, BS2013CL020, BS2014CL012).

References

[1] H. Tong, S. X. Ouyang, Y. P. Bi, N. Umezawa, M. Oshikiri and J. H. Ye, *Adv. Mater.*, 2012, **24**, 229.

[2] Z. P. Li, Q. Q. Zhao, W. L. Fan and J. H. Zhan, *Nanoscale*, 2011, **3**, 1646.

[3] F. E. Osterloh, *Chem.Soc.Rev.*, 2013, **42**, 2294.

[4] H. R. Kim, A. H. Haensch, I. D. Kim, N. Barsan, U. Weimar and J. H. Lee, *Adv. Funct. Mater.*, 2011, **21**, 4456.

[5] Z. C. Zhang, B. Xu and X. Wang, *Chem. Soc. Rev.*, 2014, **43**, 7870.

[6] Y. Liu, Y. Jiao, Z. L. Zhang, F. Y. Qu, A. Umar and X. Wu, *ACS Appl. Mater. Interfaces*, 2014, **6**, 2174.

[7] D. J. Yang, H. W. Liu, Z. F. Zheng, Y. Yuan, J. C. Zhao, E. R. Waclawik, X. B. Ke and H. Y. Zhu, *J. Am. Chem. Soc.*, 2009, **131**, 17885.

[8] S. Ida, A. Takashiba, S. Koga, H. Hagiwara and T. Ishihara, *J. Am. Chem. Soc.*, 2014, **136**, 1872..

[9] H. K. Wang, K. P. Dou, W. Y. Teoh, Y. W. Zhan, T. F. Hung, F. H. Zhang, J.Q. Xu, R. Q. Zhang and A. L. Rogach, *Adv. Funct. Mater.*, 2013, **23**, 4847.

[10] W. Tian, T. Y. Zhai, C. Zhang, S. L. Li, X. Wang, F. Liu, D. Q. Liu, X. Cai, K. Tsukagoshi, D. Golberg and Y. Bando, *Adv. Mater.*, 2013, **25**, 4625.

[11] A. Thapa, J. Zai, H. Elbohy, P. Poudel, N. Adhikari, X. Qian and Q. Qiao, *Nano Res.*, 2014, **7**, 1154.

[12] B. Liang, H. Huang, Z. Liu, G. Chen, G. Yu, T. Luo, L. Liao, D. Chen and G. Shen, *Nano Res.*, 2014, **7**, 272.

[13] S.M. Das and V. Jayaraman, *Prog. Mater. Sci.*, 2014, **66**, 112.

[14] Q. Liu, Z. Y. Zhang, W. Y. Li, K. B. Xu, R. J. Zou and J. Q. Hua,

CrystEngComm, 2015, **17**, 1800.

[15] P. Manjula, R. Boppella and S. V. Manorama, *ACS Appl. Mater. Inter.*, 2012, **4**, 6252.

[16] Y. T. Han, X. Wu, G. Z. Shen, B. J. Dierre, L. H. Gong, F. Y. Qu, Y. Bando, T. Sekiguchi, F. Filippo, and D. Golberg, *J. Phys. Chem. C*, 2010, **114**, 8235.

[17] H. Huang, H. Gong, C. L. Chow, J. Guo, T. J. White, M. S. Tse, O. K. Tan, *Adv. Funct. Mater.*, 2011, **21**, 2680.

[18] S. A. Chen, M. Wang, J. F. Ye, J. G. Cai, Y. R. Ma, H. H. Zhou and L. M. Qi, *Nano Res.*, 2013, **6**, 243.

[19] Y. Guan, D. Wang, X. Zhou, P. Sun, H. Wang, J. Ma and G. Lu, *Sensor Actuat. B-Chem.*, 2014, **191**, 45.

[20] X. X. Xu, J. Zhuang and X. Wang, *J. Am. Chem. Soc.* **2008**, *130*, 12527-12535, 2008, **130**, 12527.

[21] X. Wang, H. Fan and P. Ren, *Colloid. Surfaces A: Physicochem. Eng. Aspects*, 2012, **402**, 53.

[22] S. Zhang, P. P. Zhang, Y. Wang, Y. Ma, J. Zhong and X.Sun, *ACS Appl. Mater. Inter.*, 2014, **6**, 14975.

[23] R. Berenguer, J. M. Sieben, C. Quijada and E. Morallon, *ACS Appl. Mater. Inter.*, 2014, **6**, 22778.

[24] H. Huang, S. Tian, J. Xu, Z. Xie, D. Zeng, D. Chen and G. Shen, *Nanotechnology*, 2012, **23**,105502.

[25] T. Jia, W. M. Wang, F. Long, Z. Y. Fu, H. Wang and Q. J. Zhang, *J. Phys. Chem. C*, 2009, **113**, 9071.

[26] X. H. Jia, Y. Y. Liu, X. Y. Wu, Z. Zhang, *Appl. Surf. Sci.*, 2014, **311**, 609.

[27] J. R. Huang, L. Y. Wang, C. P. Gu, M. H. Zhai and J. H. Liu, *CrystEngComm*, 2013,**15**, 7515.

[28] P. Sun, L. You, Y. F. Sun, N. K. Chen, X. B. Li, H. B. Sun, J. Ma and G. Y. Lu *CrystEngComm*, 2012,**14**, 1701.

[29] R. H. Wei, K. Du, X. Y. Gong, Q. D. Chen, Z. X. Tang, J. H. You, L. B. Li and H. B. Yang, *Appl. Surf. Sci.*,2009, **255**, 6464.

[30] Q. Shao, A. D. White and S. Jiang, *J. Phys. Chem. B*, 2014, **118**, 189.

[31] J. Zhang, J. Guo, H. Y. Xu and B. Q. Cao, *ACS Appl. Mater. Interfaces* 2013, **5**, 7893.

[32] D. X. Ju, H. Y. Xu, J. Zhang, J. Guo and B. Q. Cao, *Sensor Actuat. B-Chem.*, 2014, **201**, 444.

[33] A. Cagliani, D. M. A. Mackenzie, L. K. Tschammer, F. Pizzocchero, K. Almdal and P. Bøggild, *Nano Res.*, 2014, **7**, 743.

[34] E. R. Leite, T. R. Giraldi, F. M. Pontes and E. Longo, *Appl. Phys. Lett.*, 2003, **83,** 1566.

[35]. L. J. Bie, X. N. Yan, J. Yin, Y. Q. Duan and Z. H. Yuan, *Sensor Actuat. B-Chem.*, 2007, **126**, 604.

[36] D. E. Williams, *Sensor Actuat. B-Chem.*, 1999, **57**,1-16.

[37] Z. F. Dai, L. Xu, G. T. Duan, T. Li, H. W. Zhang, Y. Li, Y. Wang, Y. L. Wang and W. P. Cai, *Sci. Rep*., 2013, **3**, 1669.

[38] J. Li, Y. J. Lu, Q. Ye, M. Cinke, J. Han and M. Meyyappan, *Nano Lett.*, 2003, **3**, 929.

[39] S. Thirumalairajan, K. Girija, V. R. Mastelaro and N. Ponpandian, *ACS Appl. Mater. Inter*., 2014, **6**, 13917.

[40] N. D. Khoang, D. D. Trung, N. V. Duy, N. D. Hoa and N. V. Hieu, *Sensor Actuat. B-Chem.*, 2012, **174**, 594.

[41] D. J. Yang, I. Kamienchick, D. Y. Youn, A. Rothschild and I. D. Kim, *Adv. Funct. Mater.*,2010, **20**, 4258.

[42] D. X. Ju, H. Y. Xu, Z. Qiu, J. Guo, J. Zhang, B. Y. Cao, *Sensor Actuat. B-Chem.* 2014, **200**, 288-296.

[43] A. K. Swarnaka, S. G. Huang, O. Vander Biest and J. Vleugels, *J. Alloy Compd*., 2010, **499**, 200.

[44] Z. Li, Y. Zhou, T. Yu, J. Liu and Z. Zou, *CrystEngComm.*, 2012, **14**, 6462-6468.

[45] Q. Q. Zhao, D. X. Ju, X. L. Deng, J. Z. Huang, B. Q. Cao and X. J. Xu, *Sci. Rep.*, 2015, 5, 7874.

[46] H. Zeng, W. Cai, P. Liu, X. Xu, H. Zhou, C. Klingshirn and H. Kalt, *ACS Nano*., 2008, **2**, 1661.

[47] S. M. Sun, W. Z. Wang, D. Jiang, L. Zhang, X. M. Li and Y. L. Zheng, *Nano Res.*, 2014, **7**, 1497.

[48] Y. Jiao, Y. Liu, B. Yin, S. Zhang, F. Qu and X. Wu, *Nano Energy*, 2014, **10**, 90.

[49] X. J. Xu, X. S. Fang, T. Y. Zhai, H. B. Zeng, B. D. Liu, X. Y. Hu, Y. Bando and D. Golberg, *Small*, 2011, **7**, 445.

[50] T. Zhao, J. Zai, M. Xu, Q. Zou, Y. Su, K. Wang and X. Qian, *CrystEngComm*, 2011, **13**, 4010.

Table captions

Table 1 Comparison of ZSHAs-based sensor and other reported SnO_2-based sensors.

Sensing materials (preparation)	[ethanol/glycol](ppm)	R_a/R_g	T_{sens}(^oC)
SnO_2 quantum dots[20]	100 (ethanol)	1.2	300
SnO_2 nanotubes[31]	20 (glycol)	17.2	300
SnO_2 nanowire[40]	100 (ethanol)	2	400
Our work	100 (ethanol)	10	240
	100 (glycol)	43	

Figure Captions:

Figure 1 (a) Photograph of gas sensor made by the Zn-doped SnO_2 nanostructures and (b) electronic circuit of gas sensor measurement system. V_H is the heating voltage, R_L is a constant resistance (4.7 MΩ), V_{RL} is the voltage on R_L and V_C is the constant voltage (5 V) which is applied on the R_L and the sensor.

Figure 2 (a, b) Low and high magnification SEM images; (c) TEM image, (d) HRTEM image, (e) EDX spectra and (f) XRD pattern of ZSHAs

Figure 3 Zn-doped SnO_2 gas sensor: (a) Relationship between working temperature and response at 100 ppm glycol gas, (b) responses to glycol of different concentrations at 240 °C, (c) the log (S−1) versus log (C) plot for glycol gas and the corresponding linearly fitted results, (d) response and recovery time at 10 ppm glycol gas at the operating temperature of 240 ^oC.

Figure 4 Selectivity of Zn-doped SnO_2 sensor for different target gases at 240 °C.

Figure 5 (a) Self-degradation spectra of MB solutions irradiated using a UV lamp for different times, (b) Absorption spectra of MB solutions in the presence of Zn-doped SnO_2 architectures. (c) Comparison of photocatalytic degradation efficiencies for the self-degradation of MB and Zn-doped SnO_2 architectures; (d) Photocatalytic degradation rate of MB, MO, and RhB.

Figure 6 Schematic of the photocatalytic mechanism of the as-synthesized Zn-doped SnO_2 nanostructure.

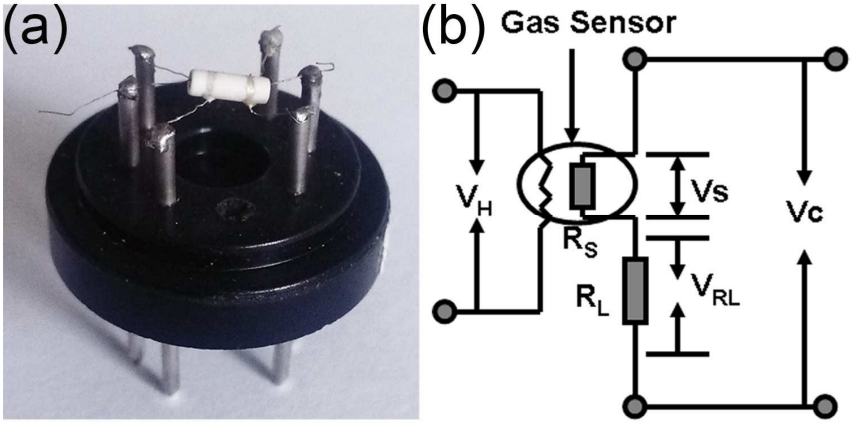

Figure 1 (a) Photograph of gas sensor made by the Zn-doped SnO_2 nanostructures and (b) electronic circuit of gas sensor measurement system. V_H is the heating voltage, R_L is a constant resistance (4.7 MΩ), V_{RL} is the voltage on R_L and V_C is the constant voltage (5 V) which is applied on the R_L and the sensor.

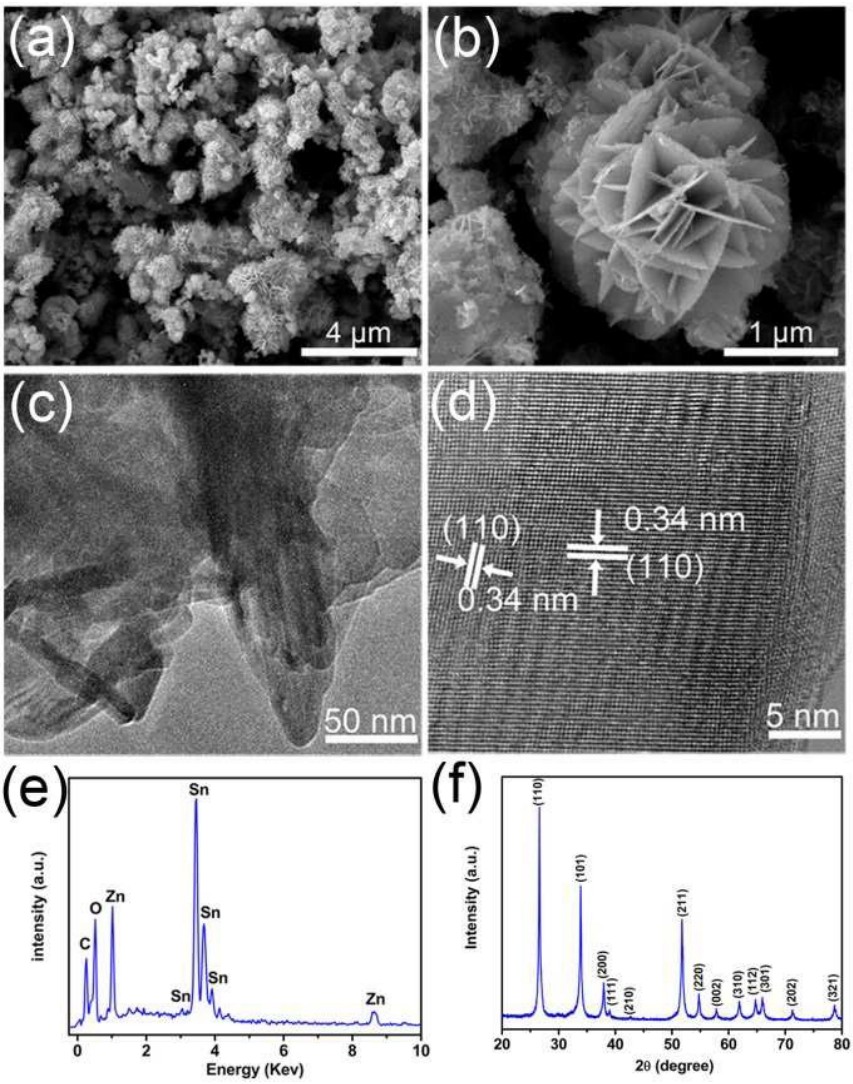

Figure 2 (a, b) Low and high magnification SEM images; (c) TEM image, (d) HRTEM image, (e) EDX spectra and (f) XRD pattern of ZSHAs.

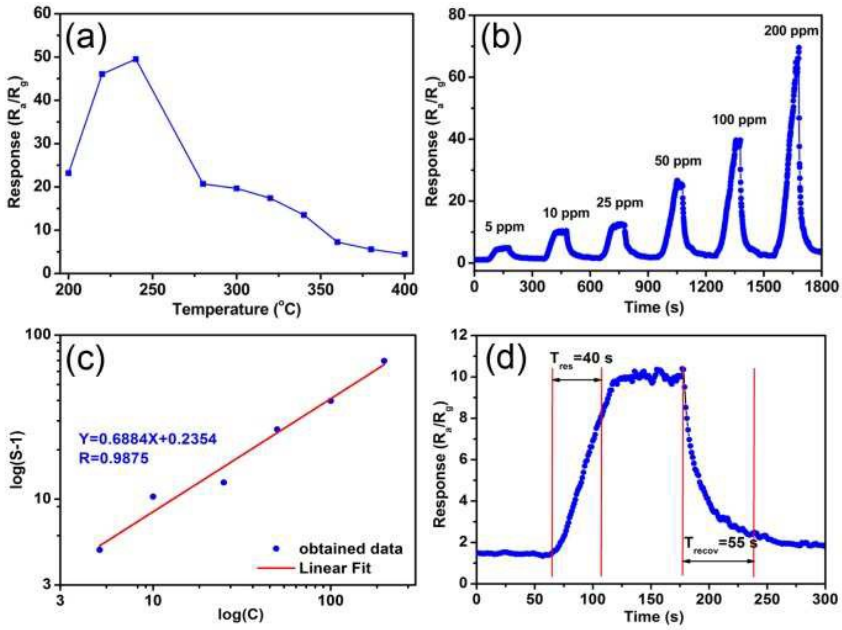

Figure 3 Zn-doped SnO_2 gas sensor: (a) Relationship between working temperature and response at 100 ppm glycol gas, (b) responses to glycol of different concentrations at 240 °C, (c) the log (S−1) versus log (C) plot for glycol gas and the corresponding linearly fitted results, (d) response and recovery time at 10 ppm glycol gas at the operating temperature of 240 °C.

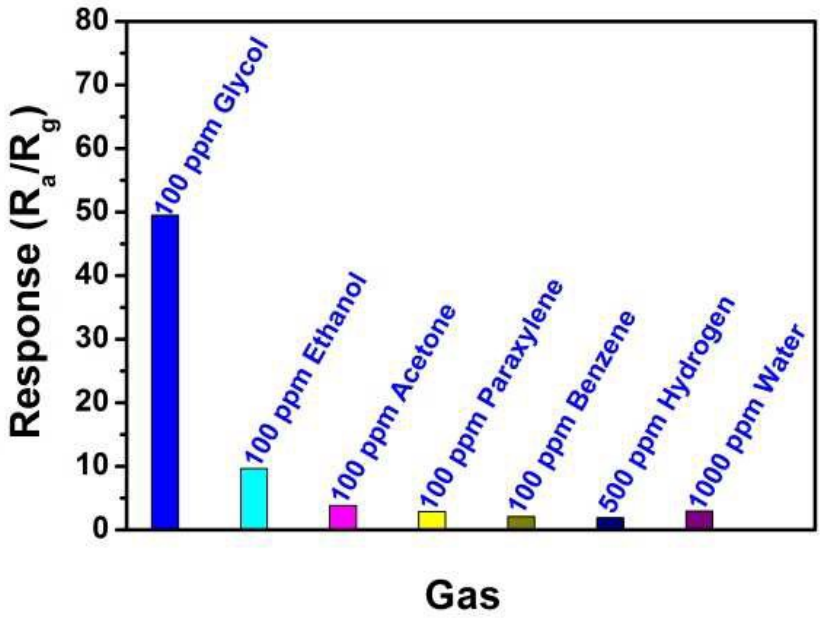

Figure 4 Selectivity of Zn-doped SnO_2 sensor for different target gases at 240 °C.

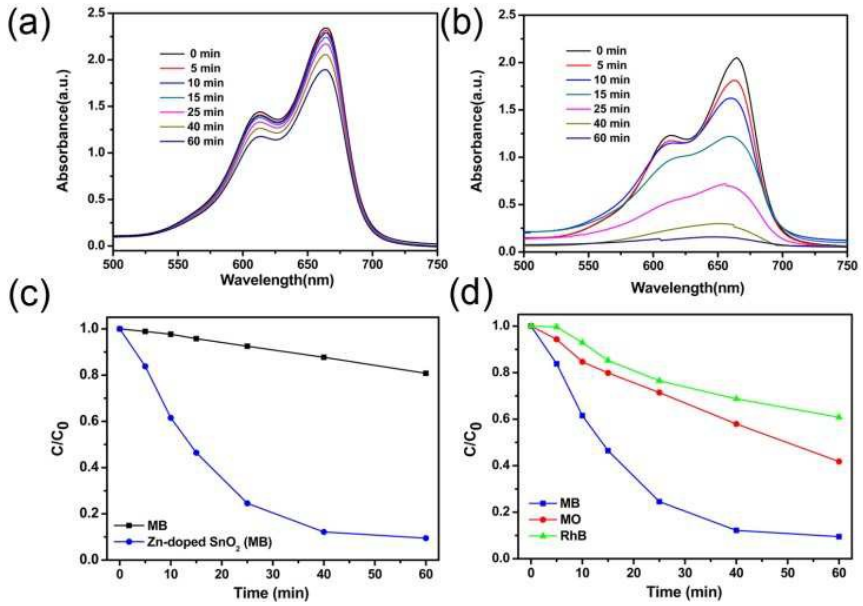

Figure 5 (a) Self-degradation spectra of MB solutions irradiated using a UV lamp for different times, (b) Absorption spectra of MB solutions in the presence of Zn-doped SnO_2 architectures. (c) Comparison of photocatalytic degradation efficiencies for the self-degradation of MB and Zn-doped SnO_2 architectures; (d) Photocatalytic degradation rate of MB, MO, and RhB.

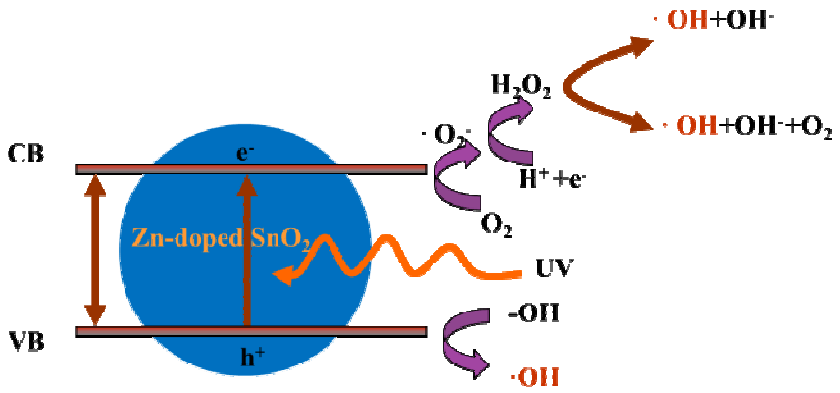

Figure 6 Schematic of the photocatalytic mechanism of the as-synthesized Zn-doped SnO_2 nanostructure.

One-pot synthesis of Zn-doped SnO_2 nanosheet-based hierarchical architectures as glycol gas sensor and photocatalyst

Qinqin Zhao[1], Xiaolong Deng[1], Meng Ding[1], Lin Gan[2], Tianyou Zhai[2], Xijin Xu[1]**

[1] School of Physics and Technology, University of Jinan, 336 Nanxinzhuang West Road, Jinan 250022, Shandong, P. R. China

[2] State Key Laboratory of Material Processing and Die & Mould Technology, School of Materials Science and Engineering, Huazhong University of Science and Technology (HUST), Wuhan 430074, Hubei, P. R. China

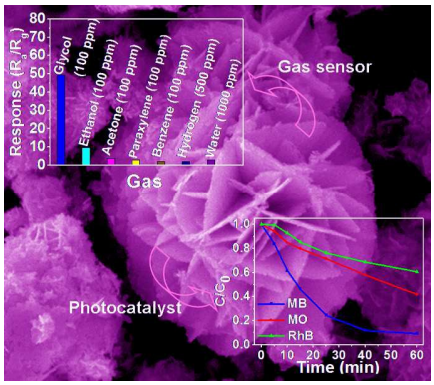

Zn-doped SnO_2 hierarchical architectures show high response and good selectivity to glycol and good selectivity to MB of photocatalyst.